Fragility Functions for Flexural Reinforced Concrete Walls

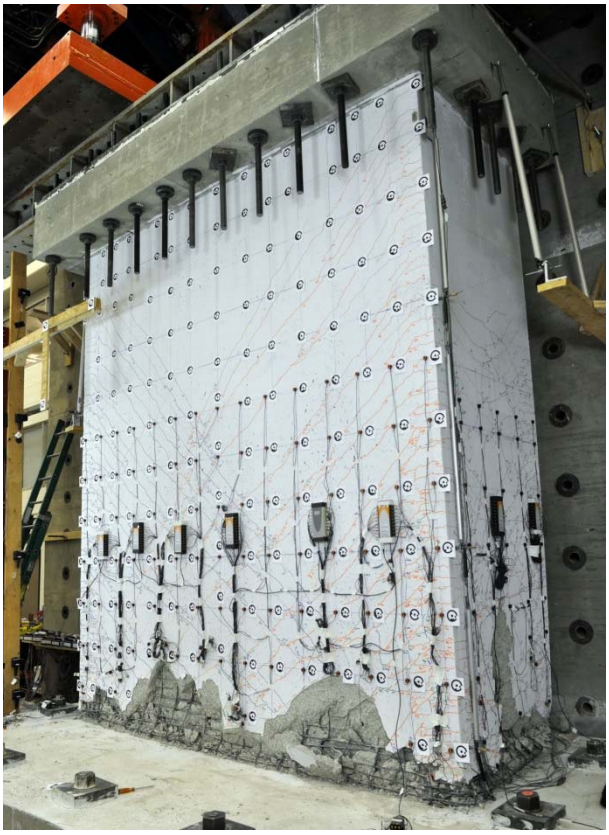

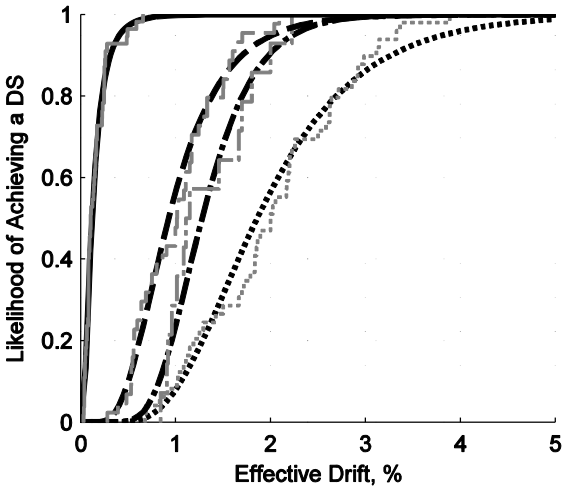

Dr. Anna C. Birely, Texas A&M University
Dr. Laura N. Lowes, University of Washington
Dr. Dawn E. Lehman, University of Washington

Funding provided by the **National Science Foundation** and the **Charles Pankow Foundation**

CHARLES PANKOW
FOUNDATION

FRAGILITY FUNCTIONS FOR FLEXURAL REINFORCED CONCRETE WALLS

Anna C. Birely, Texas A&M University
Laura N. Lowes, and Dawn E. Lehman, University of Washington

Modern seismic engineering of buildings often includes assessment of building performance for multiple levels of earthquake demand. To accomplish this assessment, performance-prediction models are required for structural components. The research presented here develops performance-prediction models for slender reinforced concrete walls, one of the most commonly used seismic-resisting systems for mid- to high-rise buildings. Performance is characterized by the *method of repair* required to restore an earthquake-damaged wall to its original performance state; commonly used methods of repair are linked directly with observed *damage states*. In recent years, a number of large-scale tests have provided extensive documentation of the progression of damage in walls subjected to simulated earthquake plus gravity loading. These tests have included walls with modern design details, with planar and flanged configurations, and representing existing construction. These data, along with data from previous tests, were assembled and evaluated to assess the impact of various design and demand characteristics on wall performance. Ultimately, data were used to develop fragility functions that define the probability that a slender wall with a given configuration will exhibit a specific level of damage and thus require a specific method of repair, given a specific level of earthquake demand.

INTRODUCTION

The seismic performance of reinforced concrete walls has been the focus of many experimental studies, likely due to the common use of structural walls as lateral systems in regions of moderate to high seismicity. The common use of walls stems from the stiffness and strength they provide in meeting service and design level criteria, the flexibility they provide in meeting architectural constraints, and the general acceptance by the engineering community that they perform well during earthquakes. Experimental research addressing reinforced concrete walls has sought to (i) advance understanding of earthquake response including the impact on earthquake response of specific design parameters (e.g. axial load, confinement, material properties, shear reinforcement, and cross-sectional characteristics such as shape), (ii) evaluate the performance of older walls and develop retrofit and/or repair techniques, and (iii) develop/validate design procedures and criteria. The results of these studies have advanced the engineering community's understanding of wall behavior and led to the current codified design procedures. Despite this, there is a need for understanding these data from a different perspective, specifically that of performance-based design and evaluation.

Performance-based seismic design and evaluation of structures seeks to design for, or determine the adequacy of a structure in meeting, specific performance objectives, where a performance objective is defined as achieving a specific performance state given a specific earthquake demand level. Structural performance is commonly defined by damage, the method of repair required to restore the damaged structure to its original performance state, and the cost and downtime associated with repair. Consequently, performance-based design and evaluation requires tools to predict damage given a measure of earthquake demand.

Fragility functions that link engineering demand parameters with the likelihood of component damage (Porter 2007) are used commonly to accomplish earthquake performance assessment.

The development of fragility functions for structural and non-structural components was a major focus of the ATC-58 project tasked with developing second-generation procedures for performance-based design of buildings (ATC 2012). In conjunction with, or complementary to, the ATC-58 effort, a number of research studies have sought to develop fragility functions for RC components, including existing beam-column joints (Pagni and Lowes 2006), modern beam-column joints (Brown and Lowes 2007), slab-column connections (Aslani and Miranda 2005) and walls (Gulec et al. 2010, Brown 2008). Gulec et al. (2010) developed fragility functions for squat walls with height to length aspect ratios of 2.0 or less; Brown (2008) developed fragility functions for walls without consideration for aspect ratio. This paper presents the results of a study to develop performance-based design tools, including fragility functions, for slender reinforced concrete walls. Results of this work are included in FEMA P-58-2 (2012).

Fragility functions are typically developed using experimental data. Wood (1991) and Fang (1992) used data from multiple experimental test programs to assess the performance of slender RC walls. However, in these previous studies, data were not evaluated with the objective of predicting the onset of specific damage states, and these studies do not include data from the many recent experimental research efforts. The current study evaluates the performance of slender RC walls using currently available sources documenting post-earthquake reconnaissance and experimental research efforts, and data are assembled with the objective of developing fragility functions for performance-based design and evaluation. Reconnaissance reports were used to identify critical damage states. Research reports were used to identify critical damage states, develop data linking demand with onset of damage states, and develop data characterizing the impact of various design parameters on damage progression.

EXPERIMENTAL DATABASE

To support development of fragility functions, an experimental database was assembled. The database comprises 78 tests from 24 research studies. Wall specimens are slender with a shear span ratio (ratio of the height of the effective shear force to the wall length) of 2.0 or greater. Individual tests were included in the database only if load-displacement response data, material properties, specimen and test set-up geometry, and specimen design parameters were available in the literature. Experiments were excluded from the database if the wall thickness was less than 50 mm (2.0 in.), openings were present in the wall, dynamic loads were applied, or lateral loading was monotonically increasing rather than cyclic. Table 1 lists the wall specimens in the database, and Table 2 provides statistics for key design and configuration properties. Birely (2012) provides a more detailed description of the wall specimens and database as well summaries of the 24 test programs.

Table 1 includes basic information about wall design, demand and failure mechanism. Table 2 includes statistics for variables characterizing wall specimen material properties, geometry,

reinforcement configuration and design. The impact on damage progression of many these variables was investigated. Variables in Table 1 and Table 2 are defined as follows.

- Shear span ratio, defined as $M/(Vl_w)$ where M is the moment at the base of the wall, V is the applied shear load, and l_w is the total length of the wall; equivalently, shear span may be defined as h_{eff}/l_w, where h_{eff} is the effective height of the applied shear load. Given the variety of specimen loading configurations (Figure 5), the shear span ratio is a more consistent measure of wall slenderness than is the ratio of wall specimen height to length.
- Compliance with the ACI 318 Code; see discussion below.
- Concrete compressive strength as measured at the time of testing, $f'_{c.}$
- Measured steel yield strength, $f_{y.}$
- Scale is defined as the lesser of 1.0 and the thickness of the web of the wall divided by 12 in.
- Wall height, h_w, is the distance from the base of the wall (top of the foundation) to the instrument used to measure lateral displacement of the wall.
- Wall length, l_w, is the length of the web of the wall; for planar walls this is the entire wall length.
- For barbell and flanged walls, t_w, is the thickness of the web of the wall, b_f is the flange width and h_f is the flange thickness.
- Boundary element length, l_b, is defined as the distance between the centers of the extreme boundary element longitudinal bars plus twice the distance from the center of the outermost bar to the center of the wall.
- Boundary element longitudinal reinforcement ratio, ρ_{be}, is defined using the boundary element area.
- Web longitudinal reinforcement ratio, ρ_{web}, is defined using the web area.
- Total longitudinal reinforcement ratio, ρ_{total}, is defined using the total wall area.
- Horizontal reinforcement ratio, ρ_h, is defined by the web thickness and the horizontal reinforcement in the web.
- Confining reinforcement ratio, ρ_{con}, is defined using the boundary element out-of-plane thickness.
- Cross-section aspect ratio, l_w / t_w.
- Boundary element length ratio, l_b/l_w.
- Out-of-plane aspect ratio, h_w/t_w.

- Maximum measured shear stress, $V_u / \left(A_{cv} \sqrt{f_c'} \right)$, where V_u is the maximum shear force applied in the laboratory and A_{cv} is the gross area of concrete carrying shear, defined per the ACI Code by the web thickness and length of the wall in the loading direction.
- Shear demand-capacity ratio, V_u/V_n, where V_u is the maximum measured shear force and V_n is the nominal shear strength calculated per Section 21.9.4.1 of the ACI Code using measured concrete and steel strengths.
- Axial load ratio, $\lambda_N = N/A_g f_c'$ where N is the applied axial load and A_g is the gross cross-sectional area of the wall.

Code compliance

Each specimen was evaluated to determine if critical seismic detailing requirements for special structural walls in Chapter 21 of the ACI Code were met. For each specimen, ACI code compliance is indicated in Table 1. In determining code compliance, several simplifications were made. First, specifications affected by specimen scaling were ignored; this included the requirement that horizontal reinforcement be spaced at less than 18 inches and boundary element confining reinforcement be spaced at less than one third the minimum dimension of the wall. Spacing requirements that are a function of reinforcing bar sizes were used in the compliance check. The need for special boundary elements was assessed using the displacement-based design approach, with a design drift of $\delta_u / h_w = 0.02$. Criteria for spacing and reinforcement areas/ratios were considered to be met if the wall designs were within 5% of the specified values. Code requirements addressing splice length, splice location and development of horizontal reinforcement were not evaluated. Finally, actual rather than specified (or design), measured material properties were used in all calculations and the ACI criteria addressing material strength were not considered.

DAMAGE STATES AND FAILURE MODES

Experimental results were analyzed to develop data linking demand with damage, failure and failure mode. Earthquake demand was quantified using deformation-based engineering demand parameters (EDPs); multiple EDPs were considered and are discussed below. Experimental data were reviewed to identify the displacement associated with the following damage: (i) initiation of concrete cracking (with distinctions made for horizontal and inclined cracks), (ii) yielding of reinforcement (as determined from moment-curvature analysis as discussed below), (iii) spalling of cover concrete, (iv) spalling exposing longitudinal reinforcement, (v) vertical cracks or splitting of concrete, (vi) boundary element core crushing, (vii) web core crushing, (viii) bar buckling, and (ix) shear failure. Economic loss is a more meaningful measure of earthquake performance for building owners that is damage. Since economic loss associated with structural damage is determined by the method of repair (MOR) required to restore a damaged component, a set of four damage states (DS) was established on the basis of associated MOR. Damage characterizing each of these four DSs and the associated MOR is provided in Table 3. For each specimen, only the minimum displacement associated with a DS was used for development of the fragility functions. Fragility functions were developed linking EDPs with the four DSs listed in Table 3.

Research results were reviewed to determine the wall specimen lateral displacement at which a particular DS initiated and at which failure initiated; multiple EDPs were then computed from this displacement. Researchers do not typically report *the* displacement at which damage occurs, but instead report that damage occurred during cycling to a maximum displacement demand. This maximum displacement demand was considered to be *the* displacement associated with onset of the damage. For specimens subjected to bidirectional loading, the minimum displacement associated with onset of a damage state was used, regardless of loading direction.

The walls in the database were tested using several different lateral load patterns; these included shear, moment and axial load applied at the top of the specimen as well as shear load only applied at the top of the specimen. To provide consistency for all load patterns, wall deformation was defined by the displacement at the effective height, h_{eff}, of the applied shear load. For the case of shear load applied at the top of the specimen, the height of the specimen and the effective height are equal ($h_{eff} = h_w$), and no modification of the measured displacement is required. For specimens subjected to other loading patterns, an elastic Timoshenko beam model was used to compute lateral displacement at the effective height given displacement and rotation at the top of the laboratory specimen. These calculations are discussed below and details are provided in Birely (2012).

There are two significant sources of uncertainty and bias in the displacement-damage data. As discussed above, *the* displacement associated with onset of a DS was typically the prescribed maximum displacement for the cyclic during which the DS initiated. This introduces uncertainty as well as an unconservative bias, since the recorded displacement is typically larger than true displacement at which damage initiated. Second, the displacement associated with *initiation* of a DS was used. Typically, initiation of a DS is reported; determining when the DS is "fully developed" requires a qualitative judgment and, thus, is not typically reported. For example, onset of bar buckling is typically reported as soon as out-of-plane movement of reinforcement is observed, even though a small amount of out-of-plane movement of the bar has minimal impact strength and likely does not require the same repair as significant out-of-plane buckling. This introduces uncertainty and a conservative bias, since reported demand values are less than those associated with "full development" of the damage state. It is not known is these two sources of uncertainty result in fragility functions that are conservative, unconservative or unbiased. The above sources of uncertainty and bias are not present in the displacement-failure data.

Moment-curvature analysis to determine yield

In Table 3, DS2 is characterized by onset of yield. However, the displacement at the onset of yield in wall longitudinal reinforcement is not consistently reported by researchers. To ensure consistent values for development of fragility functions, a wall specimen was consider to yield when the moment at the base of the wall reached the computed yield moment. Yield moment was defined by initial yield of longitudinal reinforcement and determined from a moment-curvature analysis of the wall cross section. A fiber-type model of the wall cross section and OpenSees (opensees.berkeley.edu) were used to conduct the moment-curvature analysis. For

the OpenSees analyses, concrete response was modeled using the modified Kent-Park response curve (*Concrete01* material model in OpenSees), with the strain at measured compressive strength assumed equal to -0.002 mm/mm. The impact of confining reinforcement was not considered, and concrete was assumed to have no tensile strength. The response of reinforcing steel was modeled using the OpenSees *ReinforcingSteel* uniaxial material model, which accurately represents the typical measured stress-strain response curve for reinforcing steel. If sufficient material properties were not available for calibration of the *ReinforcingSteel* model, the bilinear *Steel01* uniaxial material model was used, and, if necessary, a post-yield stiff of $0.1E_s$ was assumed.

Failure MODES

As noted above, the database assembled for this study was used to develop fragility functions predicting the onset of four DSs as well as failure. Data were assembled also to investigate the mechanism determining strength loss and failure in walls. Experimental data were reviewed and test specimens were classified as exhibiting one of the following failure mechanisms:

- Flexure-tension (FT): Drift capacity limited by fracture of the main longitudinal reinforcing bars and/or bond-slip of lap splices.
- Flexure-compression (FC): Drift capacity limited by compressive damage (bar buckling and core crushing) in boundary regions.
- Shear (S): Drift capacity limited by (a) fracture of web reinforcement, (b) diagonal shear failure, or (c) sliding shear failure.
- Web crushing (WC): Drift capacity limited by crushing of concrete in the web.

Figure 2 shows the number of specimens exhibiting each failure mechanism, with the dataset broken down by cross-section shape. Most walls exhibit flexural failure (FC or FT). Six rectangular walls failed due to shear. Six barbell and three flanged walls failed due to web crushing. More than 50% of the rectangular walls exhibited flexural-compression failures. For flanged walls, the flexural failure mode was primarily tensile (bar fracture), with the exception of a few T-shaped walls that failed due to crushing of the boundary elements, similar to the majority of the rectangular walls.

To determine if the failure modes observed in the laboratory were consistent with those observed in the field following earthquakes, a comprehensive review of post-earthquake reconnaissance reports was conducted (Birely 2012). Failure modes were identified for walls on the basis of photographs and descriptions of damage. Since field data only provide information about the damage state of the structure at the end of the earthquake, a slightly different set of failure modes defined by slightly different criteria was used for walls subjected to earthquake loading in the field:

- *Flexure-compression*: The predominant damage was spalling, bar buckling, and core crushing in the boundary region(s).*Shear - Diagonal*: Damage was predominately wide diagonal cracks.

- *Shear - Web crushing*: The predominant damage was a region of horizontal and/or diagonal crushing the wall *web*.
- *Flexure & shear - Horizontal failure plane*: Damage characterized by a horizontal region that forms an extended plane of crushed concrete, which includes both the boundary region and the web. It is difficult to know if web crushing or boundary region damage occurred first or if both occurred simultaneously. In tests conducted by Lowes et al. (2012), similar damage patterns were observed, with the region of initial damage associated w/ different mechanisms (shear or flexure) but the failure mode being the same (flexure-compression). These observations led to the creation of this category for classifying damage documented in reconnaissance reports.
- *Collapse*: Partial or complete damage of the structure (not observed in experimental tests). For structural wall buildings that collapse, the dominant type of damage, or that resulting in failure, is difficult to determine, thus such wall damage is considered independent of the above damage states.

It should be noted that the *flexure-tension* failure was not identified for walls in the field. Walls tested in the laboratory were considered to exhibit flexure-tension failure if strength loss was due to bar fracture either before or after bar buckling. However, in evaluating damage and failure of walls in the field, it was difficult to identify bar fracture from photographs and, when visible, it was not known if bar fracture resulted in significant strength loss.

Figure 3 summarizes the number of walls considered to exhibit each of the failure modes described above; walls are grouped by the region in which they were located (U.S., Chile, and other). In U.S. walls, the dominate failure mode is flexure; this is consistent with the primary failure mode in non-barbell experimental wall test specimens, indicating that the experimental damage database can be expected to yield fragility functions that provide a reasonable method for identifying expected damage in U.S. walls.

ENGINEERING DEMAND PARAMETERS

Fragility functions were developed that define the likelihood that a wall subjected to a specific magnitude of an earthquake demand parameter (EDP) will exhibit a specific damage state (DS) and thus require a specific method of repair (MOR) to restore a wall to pre-earthquake strength and stiffness. The most efficient EDP minimizes the uncertainty of the fragility function. Previous research suggests that local demand parameters, such as strain, are highly uncertain and are not as efficient predictors of damage as are more global quantities such as hinge rotation and drift (Berry et al. 2008). Thus, for the current study, plastic hinge rotation and drift at the effective height of the wall were investigated as EDPs. These parameters can be computed using analysis software employed in practice, and thus could easily be employed by practitioners considering a performance-based design or evaluation. These parameters are discussed in the following sections.

Hinge Rotation

The load-deformation response of a wall may be determined using a lumped-plasticity model that includes a plastic hinge model located at the base of the wall. In this case, hinge rotation is an easily computed EDP. To investigate the efficiency of hinge rotation for damage prediction, a lumped-plasticity model of each specimen was created. The model included a nonlinear moment-rotation hinge located at the base of the wall with the remainder of the wall was assumed to be elastic (Figure 4). A plastic-hinge length of one-half the length of the wall (l_w) was used. The region of the wall above the plastic hinge was assumed to deform in both flexure and shear. An effective flexural stiffness of $0.5E_cI_g$ and an effective shear stiffness of $0.4E_cA_g$, were used for computing rotations for all damage states except initial cracking and initial yielding. For initial cracking and yielding, these effective stiffness values resulted in overly large elastic deformation and negative rotation demands, thus, for these damage states, the gross flexural stiffness, E_cI_g, was used.

Effective drift

The experimental test specimens used to create the slender wall performance database were loaded using one of three load patterns (Figure 5): (i) lateral force applied to the top of the specimen (the most common load configuration), (ii) lateral force applied at the top of the specimen and at one or more additional locations along the height of the specimen, and (iii) lateral force and overturning moment applied at the top of the specimen. For each of these patterns, the moment-shear ratio at the base of the wall may be achieved by applying a single shear load at an *effective* height, h_{eff}, above the base of the wall. The drift at this effective height is considered to be a consistent measure of earthquake demand for walls subjected to different load patterns.

For walls loaded with only a lateral force at the top of the specimen, the specimen height is equal to the effective height and, thus, the specimen drift is equal to the effective drift. For walls with other loading conditions, the drift at the effective height was calculated. To estimate the effective drift, the model shown in Figure 4 was used. The model comprised a plastic hinge, with a hinge length equal to half of the wall length located at the base of the specimen, and an elastic element, with an effective shear stiffness of $0.4E_cA_g$ and an effective flexural stiffness of αE_cI_g. For the flexural stiffness, a coefficient of 1.0 was used for cracking and initial yield and a coefficient of 0.5 was used for all other damage states.

EVALUATION OF DAMAGE PROGRESSION

A variety of design and load parameters affect the progression of damage and the onset of failure for concrete walls subjected to earthquake loading. If data from tests of walls with widely varying design and load parameters are used to create a single fragility function defining the onset of a specific damage state, the dispersion of the data will reduce the accuracy and precision of the fragility function and ultimately result in poor prediction of building performance. Thus, the EDP-DS data developed from the tests in Table 1 were evaluated to identify the design and load parameters that most significant affect damage progression. Data were grouped on the basis of axial load ratio, cross-section shape, shear-span ratio, shear stress

demand, shear demand-capacity ratio, and uni- versus bi-directional lateral load history. For each grouping and each DS, the mean and standard deviation of the data were computed and evaluated. In this paper, fragility functions are presented for data group on the basis of axial load ratio, cross-section shape, and uni- versus bi-directional loading. Evaluation of the data suggested that only axial load ratio and cross-sectional shear impact damage progression. Since an objective of this research is assessment of the impact of bi-directional loading on wall performance, fragility functions are presented also for nonplanar walls with data grouped on the basis of uni- versus bi-directional loading. It should be noted that anecdotal evidence suggests that shear demand affects damage progression in walls. This hypothesis was not supported by the data; however, it is likely that the data set was too small, with too few specimens distributed over the full range of shear demands, to fully evaluate the impact of shear demand on damage progression.

Table 4 provides statistics for EDP-DS data for all of the wall tests combined in a single group. Data for demand defined by maximum drift and maximum hinge rotation are presented. For both EDPs there is a clear increase in the median value at the onset of the DSs as the severity of damage increases. The largest separation between median drifts at the onset of damage occurs between initial cracking (DS1) and initial cover spalling (DS2). The separation between other damage states, while distinct, is not as significant and does not exceed one standard deviation. For all DSs, the dispersion is moderately large. For initial cracking (DS1), the coefficients of variation range from 0.8-0.9; for other damage states, the coefficient of variation ranges from 0.38-0.5. This suggests the potential for reducing dispersion by grouping test specimens on the basis of design or loading parameters.

Impact of Axial load on Damage Progression

It is generally understood by the engineering community that walls with lower axial loads exhibit better earthquake performance; this hypothesis is supported by the experimental data. The impact of axial load on damage progression is most distinct when the tests are divided into two groups: walls with axial load ratio $\lambda_N < 0.10$ and with $\lambda_N \geq 0.10$. Table 5 summarizes the EDP-DS combinations for these sets of walls. Note that outliers were removed from the data set using Pierce's criterion as outlined in ATC-58 (2012). The most significant impact of axial load is the reduction in both the drift and rotation EDPs for the onset of DS4 (initial bar buckling and/or concrete crushing) for walls $\lambda_N \geq 0.10$. For demand defined by drift, initial spalling (DS2) and spalling exposing longitudinal reinforcement (DS3) have a greater median for walls with $\lambda_N \geq 0.10$ than for walls with $\lambda_N < 0.10$. This is in part due to fewer data points in the $\lambda_N \geq 0.10$ subset that correspond to a wider range of axial loads, as well as the fact that no distinction is made for wall shape. If only rectangular walls are considered (see Table 6), the median EDPs at onset of all damage states is reduced for walls with $\lambda_N \geq 0.10$. Similar observations for non-planar walls (barbell and flanged) is not practical due to limited number of data points.

Impact of Wall Shape on Damage Progression

If wall shape is considered independent of axial load, there is a clear impact on the median EDPs for a given damage state. Table 7 provides median EDPs and coefficients of variation for rectangular, barbell, and flanged walls; again outliers were removed using Pierce's criterion

(ATC 58 2012). For barbell and flanged walls, there is significant separation between the median EDP at onset of each damage state and, in most cases, the data have lower coefficients of variation than do the data for all walls combined without regard to shape (Table 4). However, for rectangular walls grouped without regard to axial load ratio, the median EDPs for DS2 and DS3 are approximately the same and the coefficients of variation for most DSs are larger than those for all walls. Thus, for rectangular walls, consideration of axial load ratio is required. In most cases, median EDPs for a damage state are smallest for planar walls and largest for barbell walls.

Damage Progression for Bi-directional Loading

Ideally, an investigation of the impact of bi-directional loading on damage progression in walls would (1) employ a dataset comprising tests of nominally identical flanged walls subjected to uni-directional and bi-directional load histories and (2) would consider damage progression in asymmetric and symmetric walls separately. In recent years a number of experimental tests of flanged walls have employed bi-directional lateral loading (Ile and Reynouard (2005); Beyer (2008); Brueggen (2009); Lowes et al. (2013)). However, there are only two test programs in which nominally identical walls were subjected to uni-and bi-directional loading (Ile and Reynouard (2005) and Lowes et al. (2013)), and these test programs employed C-shaped walls, which are symmetric under loading in one direction and asymmetric under loading in the orthogonal direction. The investigation could have been limited to C-shape walls; however, the geometry and load patterns for the eight C-shaped walls in the data set varied widely (Figure 6). Thus, to investigate the impact of bidirectional loading on response, all flanged wall tests, including C-, T- and H-shaped walls, were used and data were grouped solely on the basis of whether a uni-directional or bi-directional load history was used.

Table 8 shows the median EDPs for each damage state for flanged walls under uni- and bi-directional loading. With the exception of initial cracking (DS1), the median EDP at the onset of the damage states are approximately equal for flanged walls subjected to unidirectional and bidirectional loading. Additionally, in most cases, the coefficients of variation of the unidirectional and bidirectional data sets (Table 8) are larger than those for the combined flanged-wall data set (Table 7). For DS1, the median EDP at onset of the damage state is substantially larger for walls subjected to bi-directional loading than for walls subjected to unidirectional loading. However, the bi-directional data set is quite small, the coefficient of variation for the DS1 data is large, and the conclusion that bi-directional loading results in the onset of damage at larger deformation demands than is observed under unidirectional loading is counter intuitive. Thus, it is not clear that the data are providing an accurate characterization of the impact of bidirectional loading on the onset of DS1. In general, the data in Table 8 suggest that bidirectional loading has minimal impact on damage progression in nonplanar walls.

DEVLOPMENT AND QUANTIFICATION OF FRAGILITY FUNCTIONS

Fragility functions, which define the likelihood that a specific method of repair will be required given a specific magnitude of engineering demand parameter, are cumulative distribution functions (CDF's) that can be either empirical or functional. Empirical CDFs are created directly

from experimental data. Functional CDFs are preferred for use in practice as they are defined by two parameters; functional parameters are easily determined from experimental data.

In this study, lognormal CDFs were used to define fragility functions. This is consistent with ATC-58 (ATC 2012). Additionally, previous researchers have shown that other distributions have not provided significant improvement over this distribution with regard to predicting earthquake damage..

The parameters of a lognormal CDF can be estimated from empirical data in two ways (Halder and Mahadevan, 2000). The first method, the Method of Moments, uses the mean and variance of the empirical data set. This introduces error associated with estimating population statistics from the sample that is the data set. The second method, the Method of Maximum Likelihood, uses a likelihood function to estimate the distribution parameters that represent the empirical values. The Method of Maximum Likelihood results in a CDF that more accurately represents the empirical data, but is more sensitive to outliers. In this study, the Method of Maximum Likelihood was used to determine the parameters of the lognormal CDF's, with outliers removed as discussed in the previous section.

The experimental data were used to develop fragility functions for the subsets of walls summarized in Tables 4-8: (i) all walls with $\lambda_N < 0.10$ and $\lambda_N \geq 0.10$, (ii) rectangular walls with $\lambda_N < 0.10$ and $\lambda_N \geq 0.10$, (iii) rectangular, barbell, and flanged walls, and (iv) flanged walls under uni- and bi-directional loading. For each group, a set of fragility functions was developed for drift at effective height, and rotation demand. For each set of fragility functions, the parameters for a lognormal CDF were estimated for the DS-MOR combinations provided in Table 3. Outliers were removed from the data using Pierce's criterion outlined by ATC-58 (2012).

Tables 9-12 provide the estimated parameters for each CDF. The parameter θ is the median of the lognormal distribution and is equal to e^{μ}, where μ is the mean of the normal distribution. The parameter β_d is the dispersion and can be approximated as σ, the standard deviation of the normal distribution. The dispersion is a measure of uncertainty of the data, which can include the uncertainty of the experimental data (β_d) and uncertainty that the experimental tests represent the conditions of a real building component (β_u). The ATC-58 guidelines require that both types of uncertainty be accounted for through the following relationship:

$$\beta = \sqrt{\beta_u^2 + \beta_d^2} \tag{1}$$

The β value is not provided, but can be calculated following the ATC-58 Guidelines, which specify that the value of β_u is equal to 0.10, unless five or fewer data points were available, in which case the value is equal to 0.25.

Figure 7-9 shows the empirical and functional CDFs for each suite of fragility functions. The functional CDFs representation of the empirical CDFs, including if the chosen distribution is appropriate, was evaluated using goodness-of-fit tests. Multiple goodness-of-fit tests can be

used (Pagni and Lowes, 2006). Here, the Lilliefors test was used, which evaluates the maximum difference between the empirical and functional CDFs, represented by D_n, and compares it to tabulated values, D_n^{α} for a given significance level α (5% in this study). Table 6 provides the results of the Lilliefors test for each functional CDF, where $p = P(D_n \le D_n^{\alpha}) = 1 - \alpha$. For values of $p > 0.05$, the lognormal distribution is considered appropriate. Tables 9-12 indicate that a lognormal distribution is appropriate for most of the fragilities developed.

The fragility function parameters provided in Tables 9-12 and shown in Figures 7-9 are considered appropriate for use in PBEE of slender reinforced concrete walls; however, the appropriate fragilities to use and confidence in accuracy will depend on the application. For example, use of the wall-shape suite of fragility functions provides increased accuracy in prediction of damage. Additionally, if the axial load ratio for a wall is known, fragility functions categorized based on axial load will improve accuracy of the predictions. In the case of fragility functions for flanged walls, the use of fragilities developed from unidirectional and bidirectional nonplanar wall tests is appropriate, as the data do not indicate that lateral load direction has a significant impact on damage progression. In some cases, the fragilities shown in Figures 7-9 and defined in Tables 9-12 exhibit crossover, where for a given level of demand, onset of a more severe DS has a higher probability than does onset of a less severe DS. This results from large dispersion in the data. ATC 58 (2012) provides a procedure for correcting the fragilities in which the probability of the less severe DS is increased to match that of the more severe DS.

SUMMARY AND CONCLUSIONS

Walls are commonly used at the primary lateral-load resisting element in low to high rise structures. There is an interest in modern seismic design in developing methods to assess the performance of these elements, to better assess the performance of the building. The research study presented in this paper was conducted to both (1) understand the impact of wall design and loading characteristics on the progression of damage in walls and (2) develop fragility functions to conduct performance analyses.

To support these tasks, a large database was developed on slender structural walls. The database included 78 wall specimens. Documented information included specimen properties, measured strengths and drifts, and documented damage states. Failure modes were compared to those documented in post-earthquake reconnaissance reports to confirm the wall damage database was representative of the performance of walls in U.S. buildings.

Experimental data were reviewed to determine the design and loading parameters that have a significant impact on damage progression in the laboratory. Ultimately, suites of fragility functions were developed for (i) all walls with $\lambda_N < 0.10$ and $\lambda_N \ge 0.10$, (ii) rectangular walls with $\lambda_N < 0.10$ and $\lambda_N \ge 0.10$, and (iii) rectangular, barbell, and flanged walls. Improved accuracy in prediction of performance can be achieved if fragilities for known wall axial load or cross-section shape are used. Damage progression was found to be essentially identical for flanged walls subjected unidirectional and bidirectional load patterns. The set of fragility curves were intended to predict all salient damage states, including spalling and bar damage. For each

group, fragility functions were developed that relate the likelihood of damage to engineering demand parameters of drift and rotation demand. The resulting functions can be used in practice to predict wall damage, and therefore required repair.

It is important to note that the fragility functions presented here are based on the available experimental data for the progression of damage in slender reinforced concrete walls. Other wall characteristics and/or groupings not presented here may also significantly impact the progression of damage in walls, and with additional experimental data in the future would warrant the development of revised fragility functions. This is particularly the case for walls with high axial loads, flanged walls, and walls with bi-directional loading.

ACKNOWLEDGEMENTS

The research presented herein was funded by the National Science Foundation through the Network for Earthquake Engineering Simulation Research Program, Grant CMS-042157 and CMMI-0927178, Joy Pauschke, program manager. Any opinions, findings, and conclusions or recommendations expressed in this material are those of the authors and do not necessarily reflect the views of the National Science Foundation.

REFERENCES

Ali, A., 1990. *Reinforced concrete structural walls with staggered opening configurations under reversed cyclic loading*, Ph.D. Thesis, University of Michigan.

ATC-58, 2012. *Seismic Performance Assessment of Buildings, Volume 1 – Methodology (FEMA P-58-1)*, Prepared by the Applied Technology Council for the Federal Emergency Management Agency.

Berry, M.P., Lehman, D.E., Lowes, L.N. (2008). "Lumped-Plasticity Models for Performance Simulation of Bridge Columns," *ACI Structural Journal* 105(3): 270-279.

Birely, A.C., 2012. *Seismic performance of slender reinforced concrete walls*. Ph.D. Dissertation, University of Washington.

Birely, A.C., Hart, C.R., Marley, K.P., Lowes, L.N., Lehman, D.E., Kuchma, D.A., 2013. "Seismic Behavior of Modern Reinforced Concrete Structural Walls (Specimen PW1)", Network for Earthquake Engineering Simulation (distributor), Dataset, DOI:10.4231/D3BG2H95G.

Birely, A.C., Hart, C.R., Marley, K.P., Lowes, L.N., Lehman, D.E., Kuchma, D.A., 2013. "Seismic Behavior of Modern Reinforced Concrete Structural Walls (Specimen PW2)", Network for Earthquake Engineering Simulation (distributor), Dataset, DOI:10.4231/D36Q1SH1B.

Birely, A.C., Hart, C.R., Marley, K.P., Lowes, L.N., Lehman, D.E., Kuchma, D.A., 2012. "Seismic Behavior of Modern Reinforced Concrete Structural Walls (Specimen PW3)", Network for Earthquake Engineering Simulation (distributor), Dataset, DOI:10.4231/D3SQ8QH1F.

Birely, A.C., Hart, C.R., Marley, K.P., Lowes, L.N., Lehman, D.E., Kuchma, D.A., 2013. "Seismic Behavior of Modern Reinforced Concrete Structural Walls (Specimen PW4)", Network for Earthquake Engineering Simulation (distributor), Dataset, DOI:10.4231/D3NZ80P72.

Beyer, K., Dazio, A., and Priestley, M.J.N., 2008. Quasi-static cyclic tests of two U-shaped reinforced concrete walls, *Journal of Earthquake Engineering* 12, 1023-1053.

Brown, P.C., 2008. *Probabilistic earthquake damage predictions for reinforced concrete building components*, Master's Thesis, University of Washington.

Brown, P.C., and Lowes, L.N., 2007. Fragility functions for modern reinforced concrete beam-column joints, *Earthquake Spectra* 23 (2), 263-289.

Brueggen, B.L., 2009. *Performance of T-shaped reinforced concrete structural walls under multi-directional loading*, Ph.D. Thesis, University of Minnesota.

Dazio, A., Beyer, K., and Bachmann, K., 2009. Quasi-static cyclic tests and plastic hinge analysis of RC structural walls, *Engineering Structures* 31, 1556-1571.

Elnady, M., 2008. *Seismic rehabilitation of RC structural walls*, Ph.D. Thesis, McMaster University, 2008.

Fang, E., 1992. Failure modes of RC tall shear walls, in *Concrete Shear in Earthquakes*, Taylor & Francis, 125-133.

Halder, A., and Mahadevan, S., 2000. *Probability, Reliability, and Statistical Methods in Engineering Design*, John Wiley and Sons, Inc., New York.

Ile, N., and Reynouard, J.M., 2005. Behaviour of U-shaped walls subjected to uniaxial and biaxial cyclic lateral loading, *Journal of Earthquake Engineering* 9 (1), 67-94.

Jiang, H., Wang, B., and Lu, X. (2013) Experimental study on damage behavior of reinforced concrete shear walls subjected to cyclic loads, *Journal of Earthquake Engineering*, 17:7, pp. 958-971, DOI: 10.1080/13632469.2013.791895.

Khalil, A. and Ghobarah, A., 2005. Behaviour of rehabilitated structural walls, *Journal of Earthquake Engineering* **9** (3), 371-391.

Lefas, I.D., and Kotsovos, M.D., 1990. Strength and deformation characteristics of reinforced concrete walls under load reversals, *ACI Structural Journal* 87 (6), 716-726.

Lefas, I.D., Kotsovos, M.D., and Ambraseys, N.N., 1990. Behavior of reinforced concrete structural walls: Strength, deformation characteristics, and failure mechanism, *ACI Structural Journal* 87 (1), 22-31.

Liu, H., 2004. *Effect of concrete strength on the response of ductile shear walls*, Master's thesis, McGill University.

Lowes, L.N., Lehman, D.E., Kuchma, D.A., Behrouzi, A., Mock, A.W., 2013. "U-Shape Wall Summary Document," http://nees.org/resources/6841.

Lowes, L.N., Lehman, D.E., Birely, A.C., Kuchma, D.A., Marley, K.P., Hart, C.R., 2012. Earthquake response of slender planar concrete walls with modern detailing, *Engineering Structures* **43**, 31-47.

Lowes, L.N., Lehman, D.E., Birely, A.C., Kuchma, D.A., Marley, K.P., and Hart, C.R., 2011. *Behavior Analysis, and Design of Complex Wall Systems: Planar Wall Test Program Summary Document*, https://nees.org/resources/3677.

Mobeen, S., 2002. *Cyclic tests of shear walls confined with double head studs*, Master's Thesis, University of Alberta.

Morgan, B.J., Hiraishi, H., and Corley, W.G., 1986. *U.S.-Japan quasi-static test of isolated planar wall reinforced concrete structure*, Volume I and II, Technical Report, National Science Foundation.

Oesterle, R.G., Aristizabal-Ochoa, J.D., Fiorato, A.E., Russell, H.G., and Corley, W.G., 1979. *Earthquake resistant structural walls – tests of isolated walls – phase II*, Technical Report, National Science Foundation.

Oesterle, R.G., Fiorato, A.E., Johal, L.S., Carpenter, J.E., Russell, H.G., and Corley, W.G., 1976. *Earthquake resistant structural walls – tests of isolated walls*, Technical Report, National Science Foundation.

Oh, Y.-H., Han, S.W., and Lee, L.-H., 2002. Effect of boundary element details on the seismic deformation capacity of structural walls, *Earthquake Engineering and Structural Dynamics* 31, 1583-1602.

Pagni, C.A., and Lowes, L.N., 2006. Fragility functions for older reinforced concrete beam-column joints, *Earthquake Spectra* 22 (1), 215-238.

Paterson, J., and Mitchell, D., 2003. Seismic retrofit of slender walls with headed bars and carbon fiber wrap, *Journal of Structural Engineering*, 606-614.

Pilakoutas, K., and Elnashai, A. 1995. Cyclic behavior of reinforced concrete cantilever walls, part I: experimental results, *ACI Structural Journal* 92 (3), 271-281.

Riva, P., Meda, A., and Giuriani, E, 2003. Cyclic behavior of a full scale RC structural wall, *Engineering Structures* 25, 835-845.

Shiu, K.N., Daniel, J.I., Aristizabal-Ochoa, J.D., Fiorato, A.E., and Corley, W.G., 1981. *Earthquake resistant structural walls – tests of walls with and without openings*, Technical Report, National Science Foundation.

Su, R.K.L., and Wong, S.M., 2007. Seismic behavior of slender reinforced concrete shear walls under high axial load ratio, *Engineering Structures* 29, 1957-1965.

Tasnimi, A.A., 2000. Strength and deformation of mid-rise shear walls under load reversal, *Engineering Structures* 22, 311-322.

Thomsen, J.H., IV., and Wallace, J.W., 2004. Displacement-based design of slender reinforced concrete structural walls – experimental verification, *Journal of Structural Engineering* 130 (4), 618-630.

Tran, T.A. (2012). *Experimental and analytical studies of moderate aspect ratio reinforced concrete structural walls*. Ph.D. Dissertation, University of California Los Angeles.

Tupper, B., 1999. *Seismic response of reinforced concrete walls with steel boundary elements*, Master's Thesis, McGill University.

Wood, S.L., 1991. *Observed behavior of slender reinforced concrete walls subjected to cyclic loading*, in *Special Publication 127: Earthquake-resistant concrete structures inelastic response and design*, American Concrete Institute, 453-477.

FIGURES

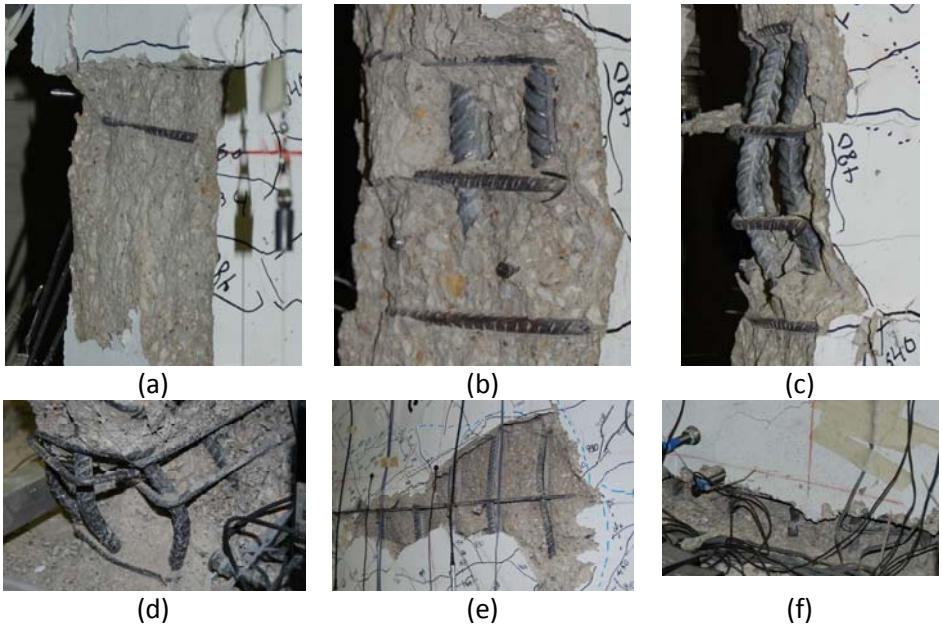

Figure 1. Selected damage states of reinforced concrete slender walls (a) cover spalling, (b) exposed longitudinal reinforcement, (c) bar buckling, (d) boundary element core crushing, (e) web core crushing, and (f) bar fracture.

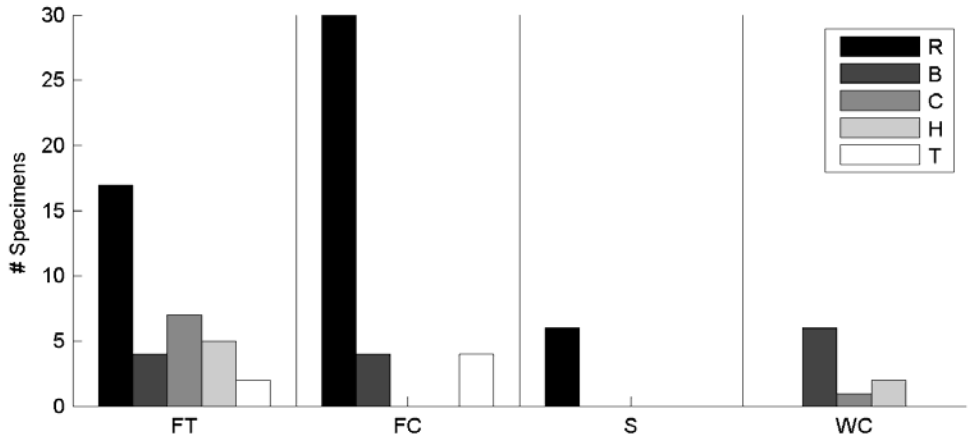

Figure 2. Summary of failure mechanisms observed in experimental tests of slender reinforced concrete wall subassemblages. Failure mode: FT = Flexure-tension; FC = Flexure-compression; S = Shear; WC = Web crushing. Shape: B = Barbell; C = C- or U-shaped; H = H- or I- shaped; R = Rectangular; T = T-shaped

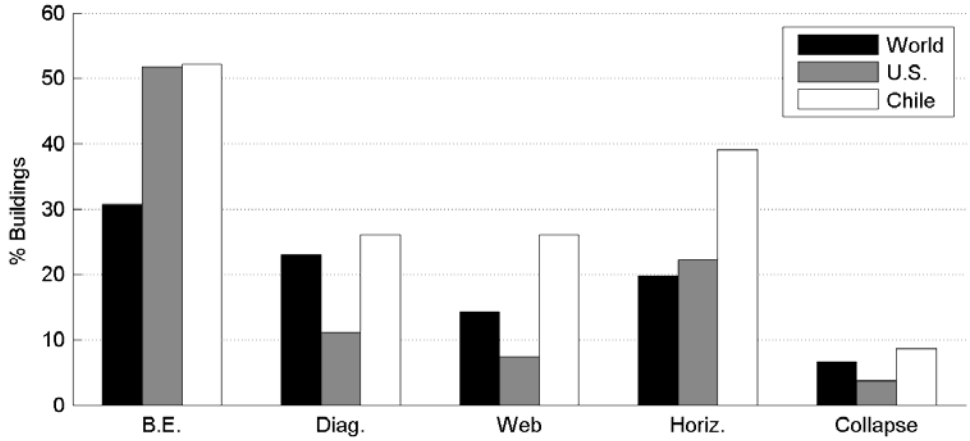

Figure 3. Percentage of total damaged wall buildings categorized with respect to predominate damage modes for buildings. For each category, comparisons are made for (i) all regions of the world, (ii) the United States, and (iii) Chile. Total may be greater than 100% due to multiple damage modes observed in the same building.

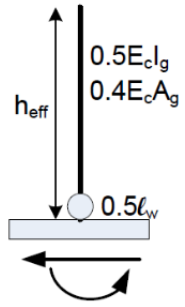

Figure 4. Model used to determine rotation demand and effective drift.

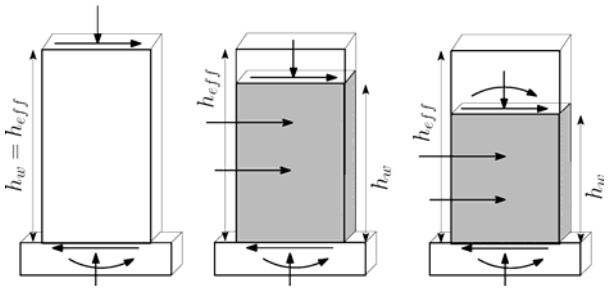

Figure 5. Categories of loading configurations.

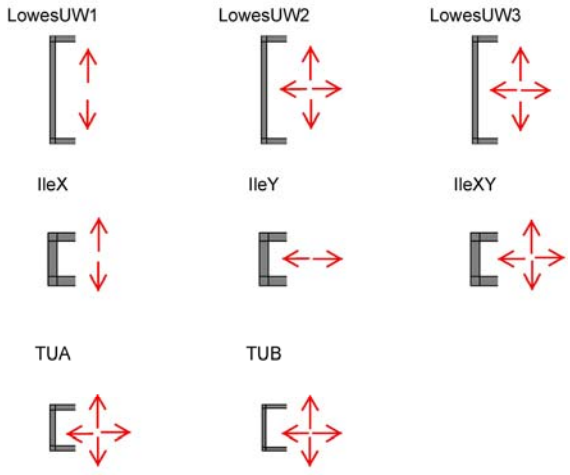

Figure 6. Loading configurations for C-shaped wall specimens.

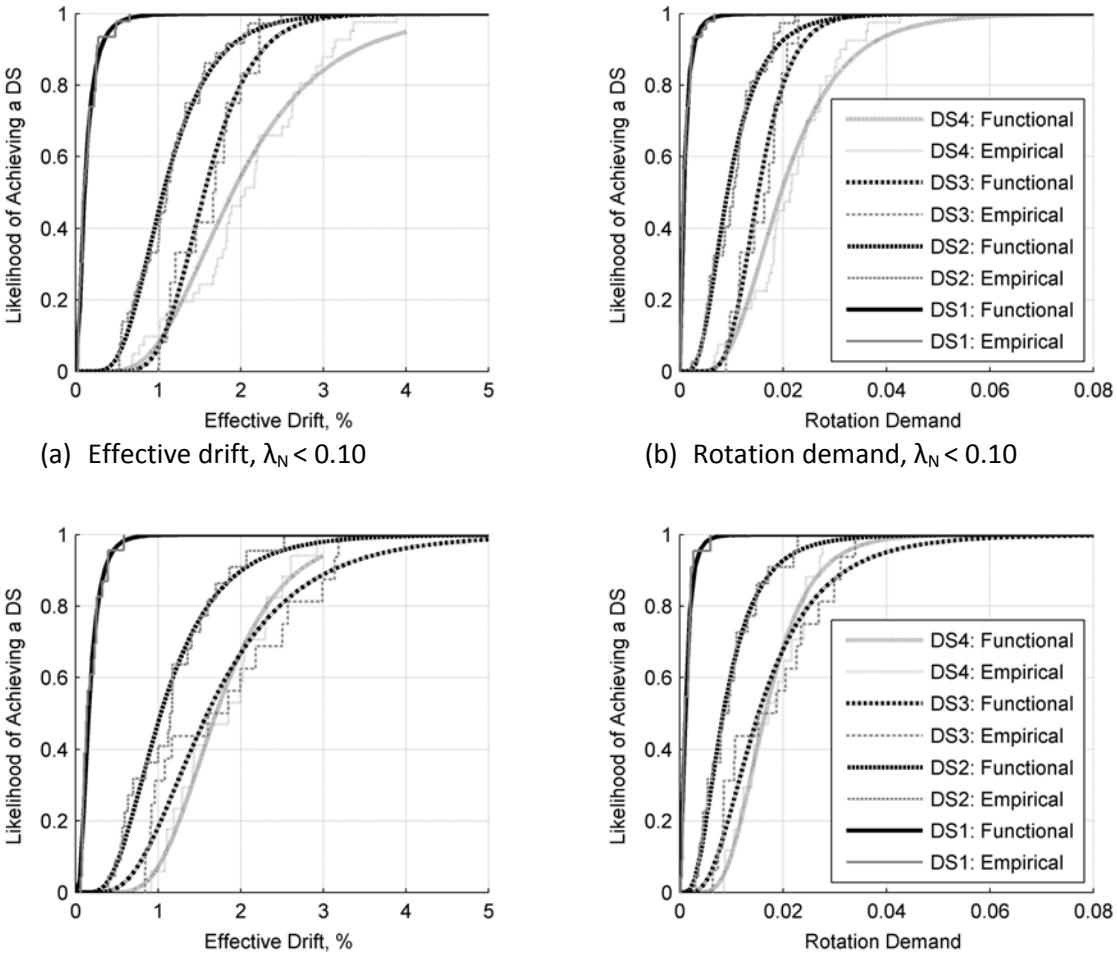

(a) Effective drift, $\lambda_N < 0.10$ (b) Rotation demand, $\lambda_N < 0.10$

(c) Effective drift, $\lambda_N \geq 0.10$ (d) Rotation demand, $\lambda_N \geq 0.10$

Figure 7. Recommended fragility functions for slender reinforced concrete walls based on axial load ratio.

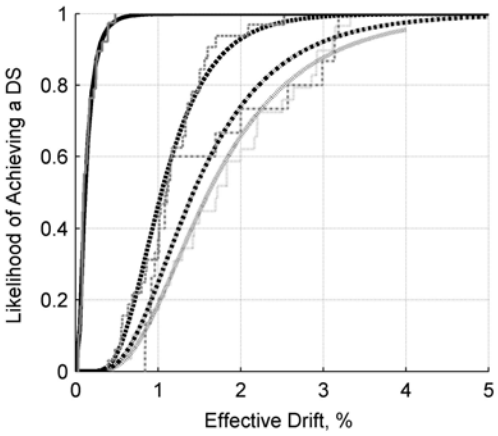

(e) Effective drift, rectangular walls

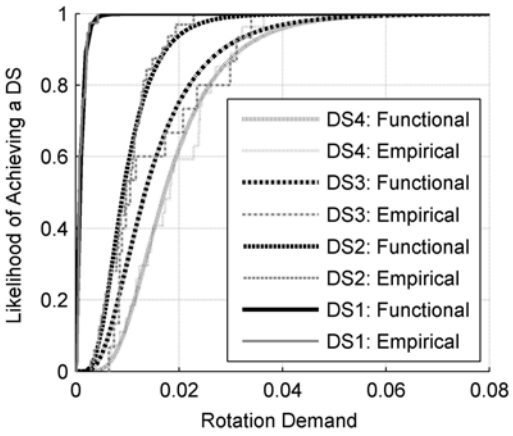

(f) Rotation demand, rectangular walls

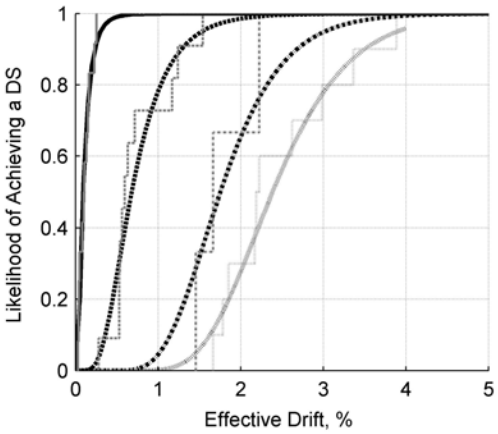

(g) Effective drift, barbell walls

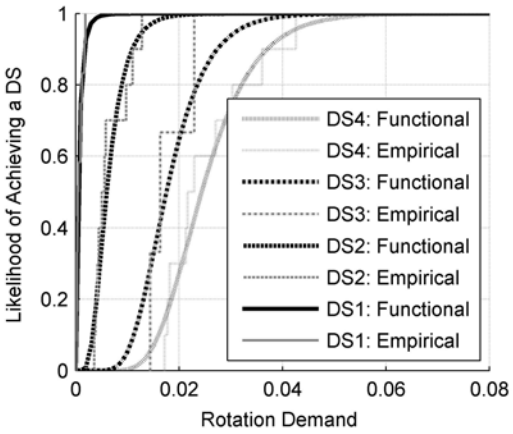

(h) Rotation demand, barbell walls

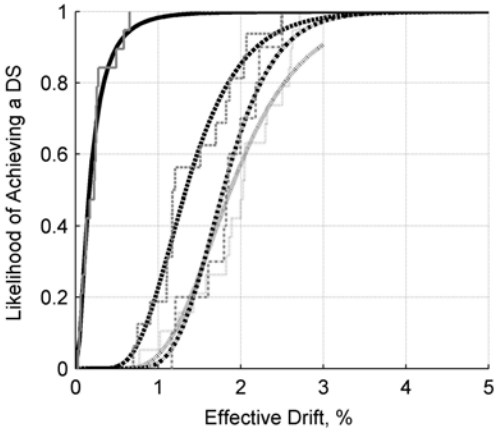

(i) Effective drift, flanged walls

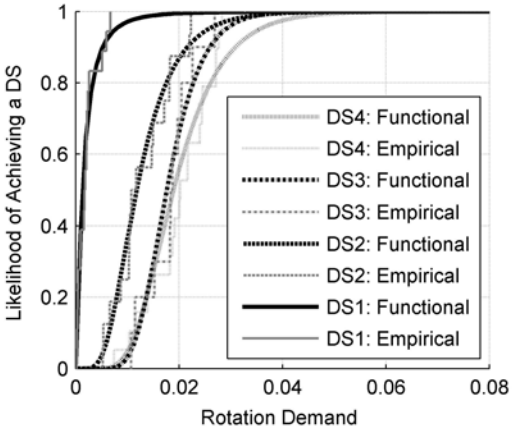

(j) Rotation demand, flanged walls

Figure 8. Recommended fragility functions for slender reinforced concrete walls based on cross-section shape.

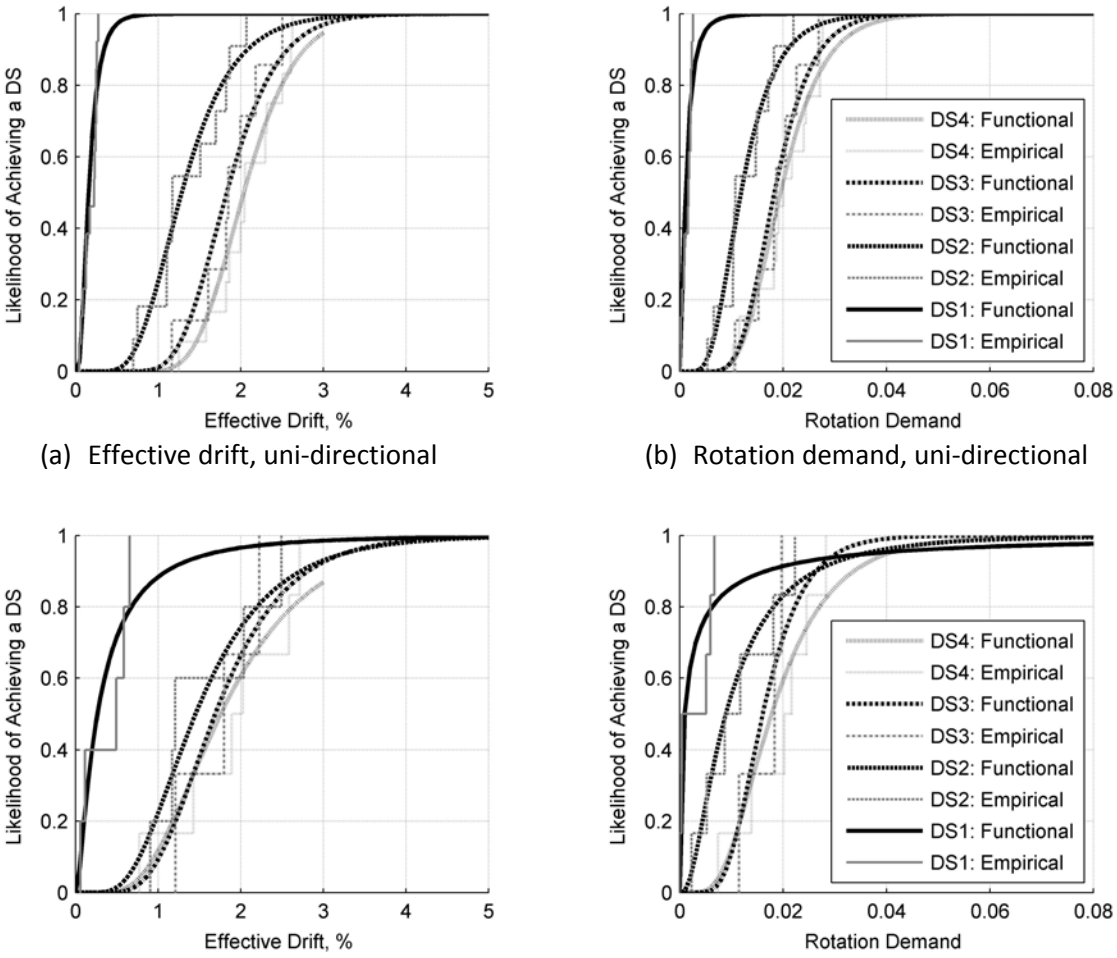

(a) Effective drift, uni-directional

(b) Rotation demand, uni-directional

(c) Effective drift, bi-directional

(d) Rotation demand, bi-directional

Figure 9. Recommended fragility functions for flanged slender reinforced concrete walls based type of loading (uni- vs. bi-directional).

TABLES

Table 1. Overview of experimental test specimens included in database.

Researcher	Name	Shape[1]	$M/(Vl_w)$	ACI Compliant	Failure Mode[2]	Max Drift %
Ali (1990)	W1	B	3.04	N	FT	3.1
Beyer et al. (2008)	TUA	C	2.58	Y	FT	3.1
	TUB	C	2.58	N	WC	2.7
Brueggen (2009)	NTW1	T	3.47	Y	FC	1.0
	NTW2	T	3.47	Y	FC	4.1
Dazio et al. (2009)	WSH1	R	2.28	N	FT	1.1
	WSH2	R	2.28	N	FT	1.4
	WSH3	R	2.28	Y	FT	2.0
	WSH4	R	2.28	N	FC	1.6
	WSH5	R	2.28	Y	FT	1.5
	WSH6	R	2.26	Y	FC	1.4
Khalil & Ghobarah (2005)	C1	R	2.25	N	S	2.6
Elnady (2008)	CW2	R	5.0	N	FT	0.2
	CW3	R	2.25	N	FT	0.3
Ile and Reynouard (2005)	X	C	2.40	N	FT	3.1
	Y	C	2.40	N	FT	3.1
	XY	C	2.40	N	FT	2.0
Jiang et al. (2013)	SW1	H	2.0	N	FT	3.1
	SW2	H	2.0	N	FT	4.1
	SW3	H	2.0	N	FT	3.4
	SW4	H	2.0	N	FT	2.5
	SW5	H	2.0	N	FC	2.9
	SW6	T	2.0	N	FC	2.2
	SW7	R	2.0	N	FC	1.5
Liu (2004)	W1	R	3.13	Y	FC	3.0
	W2	R	3.13	Y	FT	3.0
Lowes et al. (2013)	UW6	C	2.84	N	FT	2.3
	UW7	C	2.84	N	FT	1.5
	UW8	C	2.84	N	FT	1.6
Lowes et al. (2011)	PW1	R	2.85	Y	FT	1.9
	PW2	R	2.15	Y	FC	1.7
	PW3	R	2.0	Y	FC	1.3
	PW4	R	2.0	Y	FC	1.1
Mobeen (2002)	W1	B	2.74	Y	FT	3.8
Morgan et al. (1986)	W1	B	2.79	Y	FC	1.8
Oesterle et al. (1976, 1979)	R1	R	2.4	Y	FT	2.8
	R2	R	2.4	Y	FT	3.4
	B1	B	2.4	Y	FC	3.4
	B2	B	2.4	Y	WC	2.9
	B3	B	2.4	Y	FT	4.5
	B4	B	2.4	Y	FT	7.4
	B5	B	2.4	Y	WC	2.8
	B6	B	2.4	Y	WC	1.4
	B7	B	2.4	Y	WC	2.7
	B8	B	2.4	Y	WC	3.2

	B9	B	2.4	Y	WC	3.0
	B10	B	2.4	Y	FC	3.4
	F1	H	2.4	Y	WC	2.4
	F2	H	2.4	Y	WC	2.6
Oh et al. (2002)	WR-20	R	2.0	N	FC	2.7
	WR-10	R	2.0	N	FC	2.9
	WR-0	R	2.0	N	FC	2.2
	WB	B	2.0	N	FC	2.8
Paterson & Mitchell (2003)	W1	R	2.71	N	FT	0.5
	W2	R	3.13	N	FT	1.6
Paulay & Goodsir (1985)	W1	R	3.0	N	FC	2.1
	W2	R	2.6	N	FC	2.4
	W3	T	3.3	N	FC	4.3/-3.0
	W4	R	2.8	Y	FC	3.0
Pilakoutas & Elnashai (1995)	SW4	R	2.0	N	FC	2.0
	SW5	R	2.0	N	S	0.8
	SW6	R	2.0	N	FC	1.8
	SW7	R	2.0	N	S	1.8
	SW8	R	2.0	N	FC	2.2
	SW9	R	2.0	N	FC	2.2
Riva et al. (2003)	W1	R	3.17	N	S	3.2
Shiu et al. (1981)	C1	R	2.88	Y	S	2.9
Tasnimi (2000)	SHW1	R	2.2	N	FC	1.6
	SHW2	R	2.2	N	FC	1.0
	SHW3	R	2.2	N	FC	1.0
	SHW4	R	2.2	N	FC	1.7
Thomsen & Wallace (2004)	RW1	R	3.0	N	FC	1.6
	RW2	R	3.0	Y	FC	1.0
	TW1	T	3.0	N	FC	1.0
	TW2	T	3.0	Y	FC	1.7
Tran (2012)	RW1	R	2.0	Y	S	3.1
	RW2	R	2.0	Y	FC	3.0
Tupper (1999)	W3	R	3.75	Y	FC	2.9

[1] Shape: B = Barbell; C = C- or U-shaped; H = H- or I- shaped; R = Rectangular; T = T-shaped

[2] Failure mode: FT = Flexure-tension; FC = Flexure-compression; S = Shear; WC = Web crushing

Table 2. Summary of design characteristics for test specimens.

Parameters	Mean	Min.	Max.	Std. Dev.	Coeff. of Var.
f_y, ksi	67	40	87	9.3	0.14
f'_c, ksi	5.2	1.9	11.3	1.8	0.34
Scale[1]	0.40	0.2	1.0	0.17	0.44
$M/(Vl_w)$	2.5	2.0	5.0	0.52	0.21
l_w/t_w	13	6	27.5	5.0	0.36
l_b/t_w	3.3	1.0	9.0	2.5	0.77
l_b/l_w	0.2	0.10	0.5	0.13	0.54
ρ_{be}	3.4	0.8	11.4	2.2	0.65
ρ_w	0.7	0.2	2.5	0.64	0.92
ρ_t					
ρ_H	0.5	0.2	1.4	0.21	0.44
ρ_{con}	1.9	0.4	5.9	1.4	0.78
λ_N	0.1	0.0	0.3	0.08	1.07
$V_n/(A_{cv}\sqrt{f'_c})$	6.9	3.5	14.3	2.5	0.36
$V_u/(A_{cv}\sqrt{f'_c})$	5.4	1.1	17.6	3.4	0.63
V_u/V_n	0.74	0.22	1.40	0.28	0.39

[1] Scale = thickness of the wall (inches) normalized by 12 inches

Table 3. Methods of repair and associated damage states for slender reinforced concrete structural walls.

Methods of Repair		Damage State	
ID	Activities	ID	Description
MOR1	Cosmetic repair	DS1	Initial cracking and/or initial yield
MOR2	Epoxy inject cracks and patch concrete	DS2	Initial spalling
MOR3	Replace concrete	DS3	Exposed longitudinal reinforcement
MOR4	Replace wall (steel and concerte)	DS4	Core crushing; bar buckling; bar fracture; web crushing; bond slip; shear failure

Table 4. EDP statistics for damage states.

		#	Median	Std. Dev.	C.O.V.	Min.	Max.
Effective Drift	DS1	69	0.12	0.13	0.81	0.03	0.66
	DS2	59	1.12	0.51	0.45	0.28	2.53
	DS3	28	1.68	0.71	0.41	0.84	3.19
	DS4	58	2.00	0.75	0.38	0.68	3.89
Hinge Rotation	DS1	68	0.7×10^{-3}	1.3×10^{-3}	0.99	0.1×10^{-3}	6.7×10^{-3}
	DS2	59	9.8×10^{-3}	5.2×10^{-3}	0.50	2.3×10^{-3}	22.8×10^{-3}
	DS3	28	16.9×10^{-3}	7.7×10^{-3}	0.45	6.4×10^{-3}	34.0×10^{-3}
	DS4	57	20.1×10^{-3}	8.0×10^{-3}	0.39	6.5×10^{-3}	42.6×10^{-3}

Table 5. EDP medians and coefficients of variation for damage states of all walls with data grouped by axial load ration, λ_N. Outliers are removed.

		$\lambda_N < 0.10$			$\lambda_N \geq 0.10$		
		#	Median	C.V.	#	Median	C.V.
Effective Drift	DS1	46	0.10	0.88	23	0.14	0.68
	DS2	36	1.11	0.41	22	1.16	0.48
	DS3	12	1.68	0.26	16	1.73	0.49
	DS4	40	2.05	0.38	17	1.85	0.34
Hinge Rotation	DS1	46	0.7×10^{-3}	1.08	22	1.0×10^{-3}	0.85
	DS2	37	10.0×10^{-3}	0.47	22	8.9×10^{-3}	0.57
	DS3	12	16.9×10^{-3}	0.29	16	17.0×10^{-3}	0.53
	DS4	40	21.5×10^{-3}	0.39	17	17.2×10^{-3}	0.36

Table 6. EDP medians and coefficients of variation for damage states of rectangular walls with data grouped by axial load ratio λ_N. Outliers are removed.

		$\lambda_N < 0.10$			$\lambda_N \geq 0.10$		
		#	Median	C.V.	#	Median	C.V.
Effective Drift	DS1	25	0.08	0.79	13	0.14	0.64
	DS2	19	1.15	0.31	13	1.00	0.56
	DS3	5	1.15	0.31	10	1.02	0.61
	DS4	21	1.83	0.46	8	1.36	0.42
Hinge Rotation	DS1	24	0.7×10^{-3}	0.66	13	0.7×10^{-3}	0.64
	DS2	19	11.4×10^{-3}	0.34	12	7.2×10^{-3}	0.44
	DS3	5	11.7×10^{-3}	0.38	10	9.6×10^{-3}	0.67
	DS4	19	22.8×10^{-3}	0.41	8	13.1×10^{-3}	0.35

Table 7. EDP medians and coefficients of variation for damage states of rectangular, barbell and flanged walls. Outliers are removed.

		Rectangular			Barbell			Flanged		
		#	Median	C.V.	#	Median	C.V.	#	Median	C.V.
Effective Drift	DS1	38	0.10	0.74	12	0.11	0.64	19	0.23	0.78
	DS2	32	1.11	0.41	11	0.60	0.51	16	1.19	0.37
	DS3	15	1.11	0.56	3	1.67	0.22	10	1.84	0.23
	DS4	29	1.72	0.46	10	2.21	0.30	19	2.03	0.28
Hinge Rotation	DS1	38	$0.7\text{x}10^{-3}$	0.78	12	$0.5\text{x}10^{-3}$	0.80	18	$1.8\text{x}10^{-3}$	0.92
	DS2	32	$9.8\text{x}10^{-3}$	0.46	10	$5.3\text{x}10^{-3}$	0.50	16	$11.3\text{x}10^{-3}$	0.42
	DS3	15	$10.6\text{x}10^{-3}$	0.61	3	$16.4\text{x}10^{-3}$	0.25	10	$18.6\text{x}10^{-3}$	0.27
	DS4	27	$18.3\text{x}10^{-3}$	0.43	10	$22.3\text{x}10^{-3}$	0.33	19	$20.3\text{x}10^{-3}$	0.31

Table 8. Median and coefficient of variation for damage states of flanged walls with uni-directional and bi-directional loading. Outliers are removed.

		Uni-directional			Bi-directional		
		#	Median	C.V.	#	Median	C.V.
Effective Drift	DS1	13	0.23	0.45	5	0.49	0.72
	DS2	11	1.17	0.43	5	1.21	0.43
	DS3	7	1.85	0.23	3	1.80	0.29
	DS4	12	2.05	0.20	6	1.96	0.38
Hinge Rotation	DS1	13	$1.7\text{x}10^{-3}$	0.56	6	$2.8\text{x}10^{-3}$	1.01
	DS2	11	$10.8\text{x}10^{-3}$	0.40	6	$10.2\text{x}10^{-3}$	0.67
	DS3	7	$18.7\text{x}10^{-3}$	0.27	3	$18.4\text{x}10^{-3}$	0.27
	DS4	13	$20.1\text{x}10^{-3}$	0.28	6	$21.0\text{x}10^{-3}$	0.39

Table 9. Fragility function parameters and evaluation of goodness-of-fit for all walls as a function of axial load.

		$\lambda_N < 0.10$				$\lambda_N \geq 0.10$			
		θ	β_d	p	Correct CDF	θ	β_d	p	Correct CDF
Effective Drift	DS1	0.11	0.79	0.36	T	0.16	0.61	0.34	T
	DS2	1.07	0.41	0.36	T	1.03	0.51	0.18	T
	DS3	1.56	0.28	0.36	T	1.6	0.51	0.24	T
	DS4	1.9	0.45	0.04	F	1.7	0.35	0.39	T
Hinge Rotation	DS1	$0.8\text{x}10^{-3}$	0.91	0.18	T	$1.1\text{x}10^{-3}$	0.73	0.17	T
	DS2	$9.3\text{x}10^{-3}$	0.53	0.10	T	$8.4\text{x}10^{-3}$	0.58	0.5	T
	DS3	$15.2\text{x}10^{-3}$	0.31	0.34	T	$15.3\text{x}10^{-3}$	0.57	0.26	T
	DS4	$19.6\text{x}10^{-3}$	0.45	0.04	F	$16.5\text{x}10^{-3}$	0.39	0.5	T

Table 10. Fragility function parameters and evaluation of goodness-of-fit for rectangular walls as a function of axial load.

		$\lambda_N < 0.10$				$\lambda_N \geq 0.10$			
		θ	β_d	p	Correct CDF	θ	β_d	p	Correct CDF
Effective Drift	DS1	0.10	0.69	0.20	T	0.16	0.61	0.12	T
	DS2	1.14	0.32	0.49	T	0.92	0.54	0.5	T
	DS3	1.34	0.30	0.16	T	1.47	0.61	0.02	F
	DS4	1.68	0.58	0.10	T	1.44	0.37	0.14	T
Hinge Rotation	DS1	$0.7x10^{-3}$	0.62	0.08	T	$1.0x10^{-3}$	0.64	0.06	T
	DS2	$10.9x10^{-3}$	0.36	0.50	T	$6.5x10^{-3}$	0.46	0.42	T
	DS3	$13.0x10^{-3}$	0.37	0.50	T	$13.7x10^{-3}$	0.67	0.06	T
	DS4	$18.9x10^{-3}$	0.50	0.14	T	$13.7x10^{-3}$	0.33	0.5	T

Table 11. Fragility function parameters and evaluation of goodness-of-fit for barbell and flanged walls.

		All				Barbell				Flanged			
		θ	β_d	p	Correct CDF	θ	β_d	p	Correct CDF	θ	β_d	p	Correct CDF
Effective Drift	DS1	0.12	0.69	0.23	T	0.09	0.71	0.5	T	0.17	0.84	0.18	T
	DS2	1.04	0.43	0.07	T	0.68	0.48	0.18	T	1.34	0.37	0.23	T
	DS3	1.43	0.52	0.01	F	1.76	0.22	-	-	1.79	0.25	0.24	T
	DS4	1.61	0.53	0.5	T	2.40	0.28	0.32	T	1.88	0.34	0.04	F
Hinge Rotation	DS1	0.0009	0.68	.001	F	0.0006	0.86	0.5	T	0.0014	1.05	0.11	T
	DS2	0.0092	0.49	0.5	T	0.0060	0.46	0.17	T	0.118	0.46	0.5	T
	DS3	0.0134	0.58	0.12	T	0.0176	0.24	-	-	0.0176	0.29	0.08	T
	DS4	0.0172	0.48	0.25	T	0.0244	0.31	0.49	T	0.0189	0.37	0.05	T

Table 12. Fragility function parameters and evaluation of goodness-of-fit uni- and bi-directionally loaded flanged walls.

		Uni-directional				Bi-directional			
		θ	β_d	p	Correct CDF	θ	β_d	p	Correct CDF
Effective Drift	DS1	0.16	0.59	0.02	F	0.27	1.08	0.11	T
	DS2	1.29	0.36	0.5	T	1.45	0.42	0.28	T
	DS3	1.83	0.24	0.48	T	1.69	0.31	-	-
	DS4	2.04	0.22	0.5	T	1.76	0.47	0.42	T
Hinge Rotation	DS1	$1.2x10^{-3}$	0.86	0.01	F	$1.0x10^{-3}$	2.21	0.18	T
	DS2	$11.9x10^{-3}$	0.43	0.32	T	$8.9x10^{-3}$	0.84	0.5	T
	DS3	$18.3x10^{-3}$	0.30	0.49	T	$16.1x10^{-3}$	0.29	-	-
	DS4	$19.5x10^{-3}$	0.32	0.25	T	$17.8x10^{-3}$	0.49	0.18	T